PROCEEDINGS REPRINT

SPIE—The International Society for Optical Engineering

Reprinted from

Picosecond and Femtosecond Spectroscopy from Laboratory to Real World

16-17 January 1990
Los Angeles, California

Volume 1209

Picosecond photochemistry in molecular clusters

Jack A. Syage

The Aerospace Corporation
P.O. Box 92957
Los Angeles, California 90009

ABSTRACT

Rates of chemical reactions in molecular clusters were measured by picosecond spectroscopy in a molecular beam mass spectrometer. We report on two classes of reactions. First, we consider acid-base proton transfer from an aromatic species to a basic solvent cluster. The chemistry involving the aromatic acids aniline cation and S_1 phenol depended strongly on the solvent type and solvent cluster size. For example phenol*-$(NH_3)_n$ exhibited proton transfer for $n \geq 5$. The rate constant for dissociation was $k_a = (60 \pm 10 \text{ ps})^{-1}$ for $n = 5 - 7$. A geminate recombination rate of $k_{-a} = (350 \pm 100\text{ps})^{-1}$ occurs for $n = 5$. No proton transfer occurred in $(CH_3OH)_n$ solvent cluster up to $n = 11$. In another class of reactions, free radical chemistry in clusters was initiated by $\tilde{A}$ state excitation in $(CH_3I)_n$ clusters. Extensive demethylation and formation of I_2 and $I_2(CH_3I)_{n-2}$ fragments occured on the order of 10 ps. A mechanism is proposed for a chain of reactions driven in part by the energy of intracluster recombination of two CH_3 radicals and the elimination of ethane.

1. INTRODUCTION

One of the fundamental issues in reaction dynamics is understanding how solvent molecules influence the properties of a chemical reaction. This has led to investigations that compare the picosecond kinetics of gas phase reactions to that in solvents of varying viscosity.[1,2] The study of chemical reactions in molecular clusters, on the other hand, provides an exceptional medium for investigating the role of solvation on a single molecule basis. Recent studies have demonstrated that just a few solvent molecules can exert a profound influence on the energetics of both unimolecular and bimolecular reactions.[3–10] In some instances, specific solvent sizes have been identified to represent the onset of bulk-type behavior and that this critical solvent size varies in a predictable manner for different solvents. Small molecular clusters represent an uncommon state of matter that is neither gas-phase nor condensed phase.[11]

In the work presented here, we investigate the role of solvation on the course of chemical reactions by measuring changes that occur by adding solvent molecules one-at-a-time. This method is a very sensitive probe of the transition from gas-phase to condensed-phase behavior. We will examine two classes of reactions. In Sec. 3., we discuss acid-base reactions involving a proton transfer from an aromatic species to various hydrogen-bonding solvent clusters. The aromatic acids that we consider are aniline cation[7,8] and electronically excited phenol.[9] In Sec. 4, we discuss free radical reactions in clusters initiated by picosecond dissociation in $(CH_3I)_n$.[10] In each of these studies distinct reaction thresholds occur at specific solvent sizes which can be interpreted in terms of the stepwise solvation energies. These results provide us with the opportunity to systematically observe a gas phase reaction evolve toward solution phase behavior (i.e., "dissolve") on a molecule-by-molecule basis.

2. EXPERIMENTAL

2.1. Molecular Beam

The molecular beam time-of-flight (TOF) mass spectrometer is a conventional differentially pumped two chamber apparatus. Details of the vacuum system and data acquisition system have been described before.[7,8] Typical pulsed expansion conditions were 35-psi He or Ar, 500-μm nozzle diam, 400-μs pulse width, 2-cm nozzle-skimmer distance, and 1-mm diam skimmer. The ambient base pressure in the ionization chamber was typically 3×10^{-8} Torr, rising to about 2×10^{-7} Torr during operation of the pulsed nozzle at 10 Hz. The ion optics consist of the conventional three-grid configuration, as well as a pulsed electron impact (EI) ionization source described in detail elsewhere.[12–14]

Solvated aromatic clusters were prepared by a variety of procedures. In most cases, the aromatic was deposited in a sample holder contained in the temperature-controlled pulsed nozzle typically maintained at about 60 °C. In the case of ammonia sol-

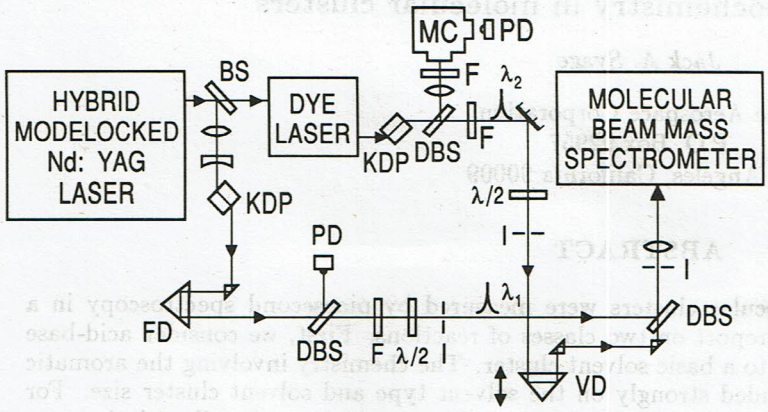

Fig. 1. A typical picosecond pump-probe configuration involving the use of Nd:YAG harmonics and a tunable dye laser. Terms are defined as follows: BS - beamsplitter; DBS - dichroic beamsplitter; F - filter; FD - fixed delay line; I - iris; $\lambda/2$ - half-wave plate; MC - monochromator; PD - photodiode; VD - variable delay line.

vation, a 2-liter high-pressure cylinder was made up containing 10% ammonia in helium. The water and methanol solvation was achieved by passing the helium flow through a bubbler containing either of these solvents. The CH_3I samples were prepared by flowing Ar (20-30 psi) through a bubbler that was cooled in a bath of dry ice/acetone or ice water, depending on the extent of clustering desired.

2.2. Cluster Ion Photodissociation

A crossed electron-laser-molecular beam configuration was used for the ion photodissociation experiments.[8,13,14] In one adaptation, neutral clusters were directly ionized by EI excitation and the cluster ions resonantly photodissociated using nanosecond laser pulses. Mass-selective photoexcitation and product ion detection was performed using a new technique in which a time-of-flight (TOF) mass spectrometer was operated as a low mass rejection filter. Details of this device are provided elsewhere,[8,14] however, the basic concept is as follows. Molecular beam ionization by EI occurs under field-free conditions in a TOF ion optics assembly. A voltage pulse is then applied to one of the grids to create a potential gradient (field) across the ionization region that is negative with respect to the direction of the detector. This accelerates the ions away from the detector with the lighter masses exiting the lower grid before the heavier masses. By reversing the field, the remaining heavier ions are accelerated toward the detector to give a TOF mass spectrum that has the primary low masses filtered out. If a delayed laser pulse is introduced after the remaining ions have turned around, then the resulting ion photofragments are detected against a zero background. Size-selected cluster ion photodissociation spectra can be derived by filtering out successively larger cluster ions before photodissociation.

2.3. Picosecond Pump-Probe

A pulsed (10 Hz) active/passive mode-locked and amplified Nd:YAG laser was used to produce frequency doubled (532 nm, 25 ps), tripled (355 nm, 25 ps), and quadrupled (266 nm, 18 ps) output, and to pump a short-cavity tunable dye laser (10 ps).[9,10] A typical optical set-up is illustrated in Fig. 1. The pump excitation was usually provided by 266 nm pulses or frequency-doubled dye laser pulses. The probe excitation was supplied by either the 532 nm or 355 Nd:YAG harmonics, or by the dye laser fundamental and/or frequency doubled output. In the latter case, the doubled Nd:YAG output (20 mJ, 25 ps, 532 nm) was split into equal portions to pump the dye laser (580-600 nm, 10 ps, 0.5-1.0 mJ) and a doubling crystal (266 nm, $\sim$ 0.4 mJ). The λ_1 and the λ_2 pulses traveled along separate variable delay lines and were then combined using a dichroic beamsplitter and directed collinearly into the molecular beam apparatus. Polarizing attenuators and neutral density filters were used to reduce pulse energies. Time-resolved spectra were recorded by delaying a probe pulse λ_2 relative to a pump pulse λ_1 using a scanning optical delay line. The nominal time resolution, as measured by the 20-80% risetime for two-color ionization was 20 ps. All traces presented were reproducible within the noise level and permitted time-constant measurements to better than 10 ps using a curve fitting and pulse-width deconvolution program.

3. ACID-BASE CHEMISTRY IN MICROSOLVENTS

Acid-base reactions are among the most fundamental in chemistry. Gas-phase[15,16] and solution-phase[16,17] studies have revealed extraordinary differences in behavior attesting to the profound effect that the solvent exerts on the properties of acid-base reac-

tions. We report results concerning the proton transfer from an aromatic species (either aniline cation or S_1 excited phenol) to a solvent cluster of varying basicity and cluster size. These reactions are particularly interesting because the dissociation is energetically unfavorable in the bare gas-phase molecule, but can become exothermic in the liquid phase. The interesting question is how large must a solvent shell be to observe an acid-base reaction.

3.1 Aniline Cation Proton Transfer

We present results for an investigation of the reactivity of a single aniline cation A^+ seeded within a solvent shell M_n of varying size (typically n = 1-10) consisting of either NH_3, N_2H_4, CH_3OH, or H_2O.[7,8] We restrict our attention to the acid dissociation yielding a proton that is mediated and solvated by the cluster M_n that surrounds the aniline amine group by hydrogen bonding.

$$C_6H_5NH_2^+ \cdot M_n \longrightarrow C_6H_5NH \cdot H^+M_n$$

$$\longrightarrow C_6H_5NH + H^+M_n. \quad (1)$$

A thermodynamic cycle appropriate to reaction (1) can be written that gives the gas phase reaction enthalpy

$$\Delta H_g = I_p(H) - I_p(A) + D_H(A\{-H\}) - D_{H^+}(M).$$

The I_p values are ionization potentials, and the D values are bond energies which are written to be interpreted as a hydrogen affinity (D_H) and a proton affinity (D_{H^+}). The addition of terms to include the energetics of stepwise solvation has been derived previously[7], and is given by

$$\Delta H_{s,n} = \Delta H_g + \sum_{i=1}^{n} \Delta E_{i,i-1}(A^+M_i) - \sum_{i=2}^{n} \Delta E_{i,i-1}(H^+M_i).$$

Here, the ΔE terms are solvation energies for successive addition of M to A^+ or H^+, respectively.

The appearance of the product H^+M_n in the REMPI mass spectra for M=NH_3, N_2H_4, and CH_3OH is presented in Fig. 2. From these and other spectra, the following observations are reached; (i) H^+M_n formed from $A^+ \cdot M_n$ precursor was observed for NH_3 and N_2H_4 with a solvent size threshold of $n \geq 3$; (ii) no protonated solvent H^+M_n was observed for CH_3OH or H_2O up to values of $n = 5$, representing the limit to acceptable signal-to-noise for these solvents.

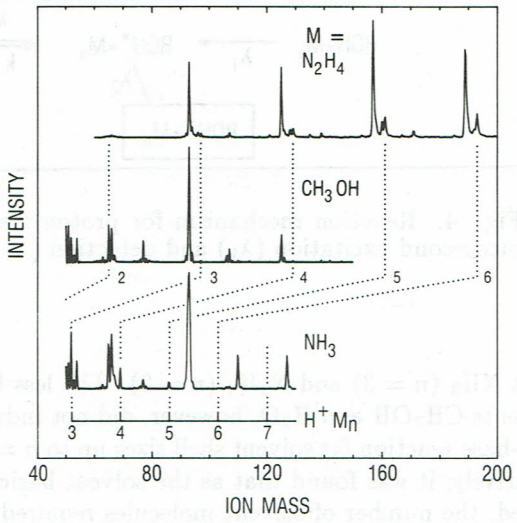

Fig. 2. 1-C REMPI/MS of A^+M_n clusters showing evidence for a critical solvent size in various solvents for dissociative proton transfer to form H^+M_n. Pulse energies were about 1.0 mJ (295 nm) for M = NH_3 and CH_3OH, and 0.40 mJ (233 nm) for N_2H_4.

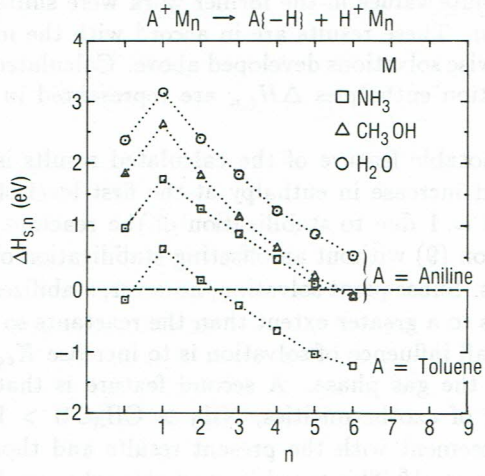

Fig. 3. Calculated stepwise solvation enthalpies as a function of solvent and shell size n for dissociative proton transfer. Calculated results are compared for A = aniline and toluene. The left-hand most data are for the gas phase reactions.

As expected, proton transfer from aniline to M_n to form H^+M_n was strongly dependent on M_n proton affinity, which for a particular solvent generally increased with n. A small solvent threshold size for formation of H^+M_n was observed for the more basic

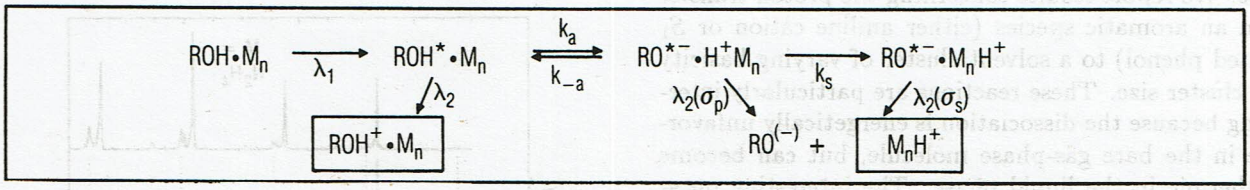

Fig. 4. Reaction mechanism for proton transfer in microsolvated phenol, and the method of picosecond excitation (λ_1) and detection (λ_2).

solvents NH_3 ($n = 3$) and N_2H_4 ($n = 2$). The less basic solvents CH_3OH and H_2O, however, did not induce an acid-base reaction for solvent shell sizes up to $n = 4$. Qualitatively, it was found that as the solvent basicity increased, the number of solvent molecules required to initiate an acid-base reaction decreased.

Brutschy *et al.*[6] recently reported evidence for a threshold solvent size effect in the dissociative proton transfer involving toluene and p-xylene solvated with NH_3, CH_3OH, and H_2O. The relative ordering of the n threshold values for the various solvents was consistent with that observed in the present work, although the absolute values in the former work were shifted to smaller n. These results are in accord with the model for stepwise solvations developed above. Calculated microsolvation enthalpies $\Delta H_{s,n}$ are represented in Fig. 3.

A notable feature of the calculated results is the predicted increase in enthalpy at the first level of solvation $n = 1$ due to stabilization of the reactant side of reaction (9) without an offseting stabilization of the products. Subsequent solvation, however, stabilizes the products to a greater extent than the reactants so that the overall influence of solvation is to increase K_{eq} relative to the gas phase. A second feature is that the ordering of exothermicities, $NH_3 > CH_3OH > H_2O$, is in agreement with the present results and those of Brutschy *et al.*[6] This trend is most strongly correlated with the proton affinity $D_{H+}(M)$. A third feature is that the calculated solvation enthalpies $\Delta H_{s,n}$ are more exothermic for A=toluene, thus explaining the smaller threshold values of n reported by Brutschy *et al.* for that system. The calculated curve for the reaction involving toluene-$(NH_3)_n$ is plotted in Fig. 3, although the calculated curves for all solvents are shifted in energy from the aniline-$(NH_3)_n$ data by essentially a constant representing the differences in the I_p and hydrogen bond dissociation energy $D_H(A\{-H\})$ of the aromatic cations.

3.2. Phenol (S_1) Proton Transfer

The use of molecular clusters is proving to be an excellent medium for studying stepwise solvation. However, the existing body of work (including the above aniline cation study) is comprised of steady-state experiments which are sensitive only to the equilibria of reactant and product. Time-resolved measurements, on the other hand, exist only for solution phase systems.[18–20] In this section, we report direct picosecond measurements of the rate constants for acid dissociation k_a and geminate recombination k_{-a} as a function of solvent cluster size for the seeded cluster system phenol-$(NH_3)_n$ (henceforth ROH·M_n).[8]

Aromatic alcohols in solution are known to be more acidic in their S_1 state than in S_0 (i.e., the so-called pH jump).[17] In the present picosecond cluster experiment, the $\lambda_1 = 266$ nm pump pulse excites the ROH·M_n clusters to S_1 with excess energy ranging from about 1900 cm^{-1} ($n = 1$) to about 2250–2800 cm^{-1} (estimated for $n = 3 - 7$).[21,22] The S_1 origin of uncomplexed phenol is at 274.7 nm.[22] A reaction mechanism modeled after solution phase behavior (described shortly) is given in Fig. 4, along with the λ_2 detection method. The excited state clusters absorb strongly at $\lambda_2 = 532$ nm to give either parent ion ROH·M_n^+ or protonated solvent M_nH^+, depending on whether a proton transfer has occurred in the excited state acid ROH*·M_n to form RO^{*-}·H^+M_n.

Figs. 5-7 consist of the time-resolved traces for the decay of undissociated acid and the formation of protonated solvent as a function of solvent cluster size M_n. The most prominent observation in Fig. 5 is the onset of ROH*·M_n reactive decay for solvent cluster $(NH_3)_n$ of size $n = 5$. No evidence for reaction was observed when phenol was seeded in the less basic solvent clusters $(H_2O)_n$ ($n \leq 5$) or $(CH_3OH)_n$ ($n \leq 11$). These results should be compared to a steady-state dispersed fluorescence experiment on the proton transfer reaction in 1-naphthol*$(NH_3)_n$, which exhibited a solvent threshold at $n = 4$ for $(NH_3)_n$ but no reaction for CH_3OH

and H_2O solvents of larger cluster size.[3] The solvated napthol reaction is about 0.3–0.5 eV less endothermic than the corresponding phenol reaction[3] and, hence, is expected to be stabilized by a smaller solvent shell. Interestingly, the enthalpy difference between naphthol and phenol is close to the expected solvation energy for a single NH_3 molecule with an ion in a small cluster, which agrees with the difference in solvent threshold size of about one.

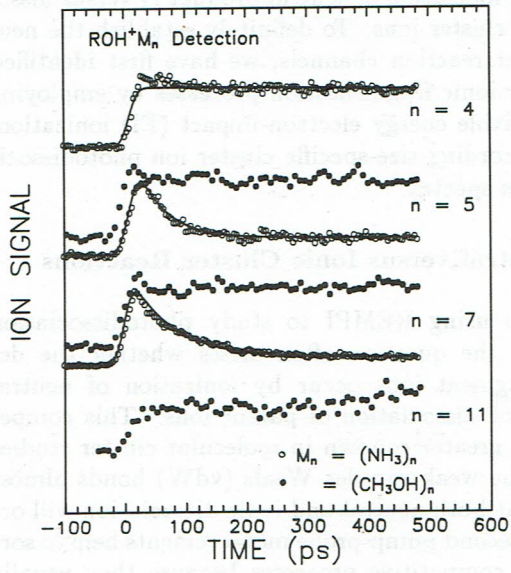

Fig. 5. Picosecond measurements for decay of reactant cluster $ROH^*{\cdot}M_n$ (as detected by $ROH{\cdot}M_n^+$). Pulse characteristics were λ_1 (266 nm, $\sim$ 20 μJ, 2 mm diam) and λ_2 (532 nm, $\sim$ 1 mJ, 3 mm diam). The calculated traces for $ROH{\cdot}M_n^+$ are based on the equilibrium model in Fig. 4 ($n = 4$ assumes $k_a = 0$).

The traces in Fig. 6 show that the formation rate of product M_nH^+ matches the decay rate of reactant $ROH^*{\cdot}M_n$. Also evident are longer time components (which we discuss shortly). The results using $\lambda_2 = 532$ nm indicate that the M_nH^+ product signal has suffered evaporation of two NH_3 molecules. This is evident by the appearance of a finite rise-time due to proton transfer at $n \geq 3$. For $\lambda_2 = 355$ nm, proton transfer appears only for $n \geq 4$, indicating evaporation of at most a single solvent molecule. These results are explained by the greater excess energy that occurs by two-photon ionization at 532 nm than by one-photon ionization at 355 nm. Some evaporation probably occurs in $ROH{\cdot}M_n^+$ as well; however, because the parent cluster distribution decreases with n, fragmentation of larger parent cluster ions does not interfere with the signals for the smaller cluster ions, unlike for M_nH^+ production which increases with n.

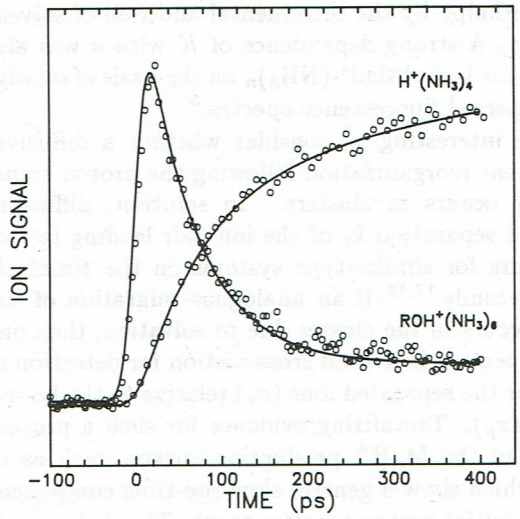

Fig. 6. Representative traces for reactant cluster $ROH^*{\cdot}M_n$ (as detected by $ROH{\cdot}M_n^+$) and product $RO^{*-}{\cdot}H^+M_n$ (as detected by M_nH^+) showing the same 65 ± 10 ps time-constant for proton transfer.

The time-resolved transients conform remarkably well to the mechanism for intermolecular proton transfer in solution.[17–20] We therefore use this description as a consistent (but not necessarily unique) model for the microsolvation cluster results.[8] We call attention in particular to the following observations: (1) the trace for $n = 5$ decays to a distinct plateau; (2) the decay time for $ROH^*{\cdot}M_n$ does not vary greatly for $n \geq 5$; (3) the production of M_nH^+ is not described by a single exponential time-constant. The reaction mechanism portrayed in Fig. 4 considers a fast acid-base equilibrium defined by the acid dissociation and geminate recombination rate constants (i.e. $K = k_a/k_{-a}$) and a slower diffusion-controlled rate constant k_s for separation of the ion-pair to form free ions (i.e., cage escape). For small solvent clusters, this corresponds to inclusion of a solvent molecule between the two counter-ions, which we denote by $RO^{*-}{\cdot}M_nH^+$ in Fig. 4.

The time-dependence for reactant $ROH^*{\cdot}M_n$ $n = 5$ in Fig. 5 is indicative of an acid-base equilibrium. This assumption leads to calculated best fit rate constants of $k_a = (60 \pm 10 \text{ ps})^{-1}$ and $k_{-a} = (350 \pm 100 \text{ ps})^{-1}$. The rate constant for dissociation k_a does not vary much for values of n larger than the critical solvent size [$k_a \sim (65 \text{ ps})^{-1}$ for $n = 6, 7$]. On the other hand, K changes dramatically in the solvent threshold region $n = 4 - 6$. This behavior occurs because the solvent stabilizes the product ion-pair state to a much greater extent than the reactant neutral excited state.[16] As a result, the activation energy is rather insensitive to n, whereas relatively large changes take place in the re-

action enthalpy by the incremental addition of solvent molecules. A strong dependence of K with n was also reported for 1-naphthol*-$(NH_3)_n$ on the basis of steady-state dispersed fluorescence spectra.[3]

It is interesting to consider whether a diffusive-type solvent reorganization following the proton transfer event occurs in clusters. In solution, diffusion-controlled separation k_s of the ion pair leading to free ions occurs for similar-type systems on the timescale of nanoseconds.[17,19] If an analogous migration of the proton occurs in the cluster due to solvation, then one might expect an increased cross-section for detection of M_nH^+ for the separated ions (σ_s) relative to the bound ion-pair (σ_p). Tantalizing evidence for such a process is found in the M_nH^+ production curves, such as in Fig. 7, which show a general slow-rise-time component after the initial proton transfer event. This behavior is found for all solvent cluster sizes n that show proton transfer and is observed for both $\lambda_2 = 532$ nm and 355 nm. Calculated traces reveal that the formation curves for M_nH^+ fit well to a biexponential function with a long-time component of 2 ns (cf. Fig. 7., $n = 4$, solid line). Also shown is a calculated curve that assumes $k_s = 0$.

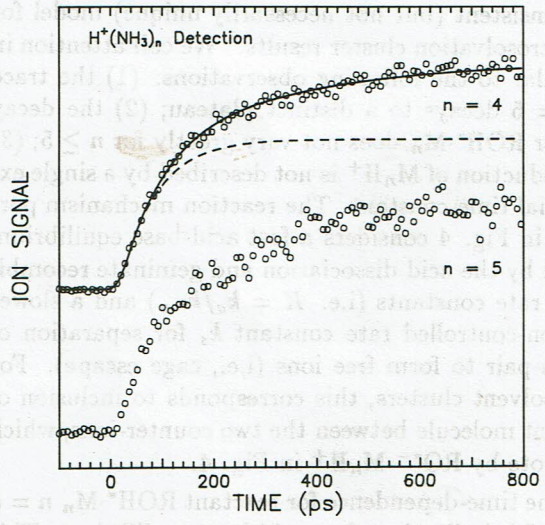

Fig. 7. Picosecond measurements for formation of product $RO^{*-}\cdot H^+M_n$ (as detected by M_nH^+). The best fit calculation for M_nH^+ $n = 4$ (—) is for $k_a = (70\text{ ps})^{-1}$, $k_s = (2.0\text{ ns})^{-1}$, and $\sigma_s/\sigma_p = 3.8$. A calculation for $k_s = 0$ is also shown (- - -).

4. FREE RADICAL CHEMISTRY IN $(CH_3I)_n$ CLUSTERS

In this section, we present picosecond measurements of reactions in $(CH_3I)_n$ clusters.[10] The photoreactions were initiated by exciting into the directly dissociative $\tilde{A}$ state. The monomer reaction dissociates into CH_3 + I in less than 1 ps,[23] however for certain cluster sizes one can expect sufficient caging of the initially formed radicals to induce chemistry within the cluster. Vaida, *et al.* suggested that I_2 is produced in $(CH_3I)_n$ clusters on the basis of the detection of I_2^+ following nanosecond MPI through the valence $\tilde{A}$ state.[24] Their results, however, do not distinguish between I_2^+ formed by ionization of neutral product I_2 versus dissociation of cluster ions. To definitely establish the neutral cluster reaction channels, we have first identified the purely ionic fragmentation processes by employing direct variable energy electron-impact (EI) ionization, and by recording size-specific cluster ion photodissociation mass spectra.[8,10]

4.1. Neutral versus Ionic Cluster Reactions

When using REMPI to study photodissociation processes, the question often arises whether the detected fragment ions occur by ionization of neutral products or dissociation of parent ions. This competition is a greater concern in molecular cluster studies because the weak van der Waals (vdW) bonds almost ensure that both neutral and ionic dissociation will occur. Picosecond pump-probe measurements help to sort out these competitive processes because they usually occur over different timescales. However, we also take the independent approach of measuring directly the ion dissociation mechanisms by electron-impact (EI) ionization and by mass-selective ion photodissociation. The ion photodissociation experiments make use of a crossed electron-laser-molecular beam configuration as described in Sec. 2.2. The molecular clusters are first ionized by EI excitation, then mass filtered, and finally resonantly photodissociated using nanosecond laser pulses.[8,12,13]

The methodology behind using both REMPI and direct ionization to identify neutral cluster reactions is illustrated in Fig. 8 for $(CH_3I)_n$ clusters. The EI cluster mass spectrum in Fig. 8a shows ion fragment signals that occur exclusively by ion dissociation mechanisms. The electron beam flux is sufficiently low that all excitation events occur by a single electron. The estimated ionization probability is about 10^{-6}. Consequently, the ion signals that appear in Fig. 8a are due to parent cluster direct ionization and subsequent cluster ion dissociation. The latter process consists only of dissociation of a single C-I bond or van der Waals (vdW) evaporation. The operation of the TOF low mass rejection filter is illustrated in Fig. 8b for the rejection of all ion masses less than the dimer mass. In Fig. 8c,

low mass rejection is followed by a photodissociation pulse that is resonant with a predissociative absorption in CH_3I. The resulting mass spectrum clearly shows that only vdW dissociation occurs in the cluster ions rather than C-I bond breaking. Finally, Fig. 8d contains the picosecond REMPI mass spectrum of $(CH_3I)_n$ resulting from excitation of the dissociative $\tilde{A}$ state. A distinctly different spectrum is obtained compared to the ion fragmentation spectra in Figs 8a-c. As a result of the overall procedure encompassed by Fig. 8, the additional signals in Fig. 8d can be confidently assigned to ionization of *neutral* reaction products.

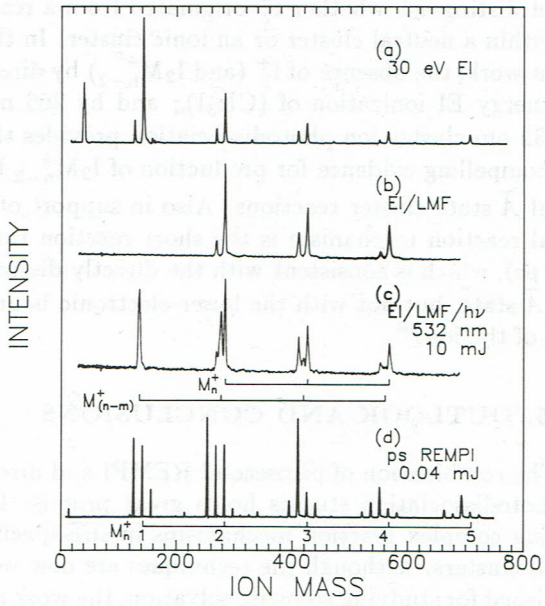

Fig. 8. $(CH_3I)_n$ cluster ionization mass spectra (M = CH_3I). (a) Direct ionization by EI excitation at 30 eV. (b) EI ionization and low mass filter (LMF). (c) Same, but with resonant photodissociation of cluster ions. (d) Picosecond $\tilde{A}$ state REMPI. Expansion conditions were 5% CH_3I in 1200 Torr Ar.

4.2. Picosecond Rate Measurements

The excited state neutral clusters undergo very rapid chemistry. Examples of picosecond pump-probe traces for some of the major products are given in Fig. 9. A more complete mapping of the product time dependence versus cluster size has been reported elsewhere.[10] The measured rates for the formation of $I_2(CH_3I)_{n-2}$ as a function of cluster size n exhibit a sharp reduction in signal at $t = 0$ and remains at a constant level to long delay times. The latter behavior suggests that dissociation takes place in the long-lived ion, presumably due to the I_2 (or I_2^+) component. However the sharp threshold with delay time indicates that the ion, and therefore the neutral product, is formed within the instrument resolution of 10 ps. Also shown in Fig. 9 is the product $I_3(CH_3I)_{n-3}$, corresponding to loss of three CH_3 groups, that opens up for cluster sizes $n \geq 4$. The ion signal undergoes a rapid depletion at $t = 0$ within the instrument response time and then recovers for $t > 0$. Because of the signal recovery, it is unlikely that the dissociation occurs in the long-lived ion, but rather in the short-lived neutral. The $I_3M_{n-3}^+$ response is strong evidence for a neutral reaction mechanism.

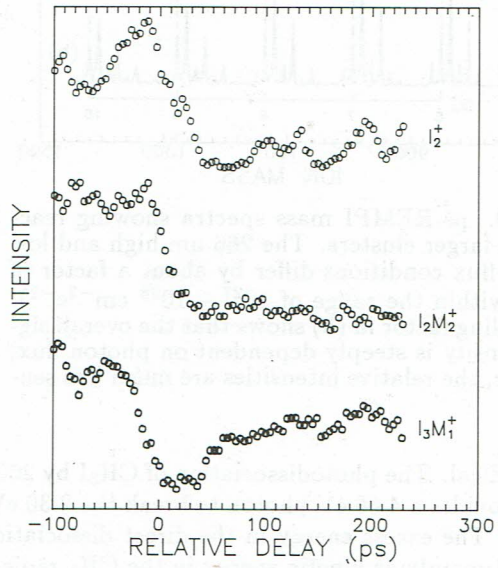

Fig. 9. Picosecond measurements using 266 nm pump and 532 nm probe: M_n (M = CH_3I) reaction for loss of two and three CH_3 groups [I_2M_{n-2} ($n = 2,4$) and I_3M_{n-3} ($n = 4$), respectively].

4.3. "Hot" Radical Reaction Mechanism

The 266 nm ps-MPI mass spectra in Figs. 8d and 10 show that the photoexcited clusters can lose a substantial fraction of the CH_3 groups allowable by cluster size. Also evident in Fig. 10 is an alternation of peak intensities separated by two CH_3 mass units. Because the product distribution is observed to shift to greater demethylation at higher pulse energies, it is believed that sequential photon absorption plays some role in demethylation. However, because demethylation is relatively extensive even at low pulse energies (Fig. 10b), it seems unlikely that sequential photon absorption can account for all the products observed. This conclusion is supported by the photon flux and absorption cross section data.[10]

The picosecond measurements and mass spectral features can be explained by a simple, but plausible reaction mechanism based on the chemistry of a "hot"

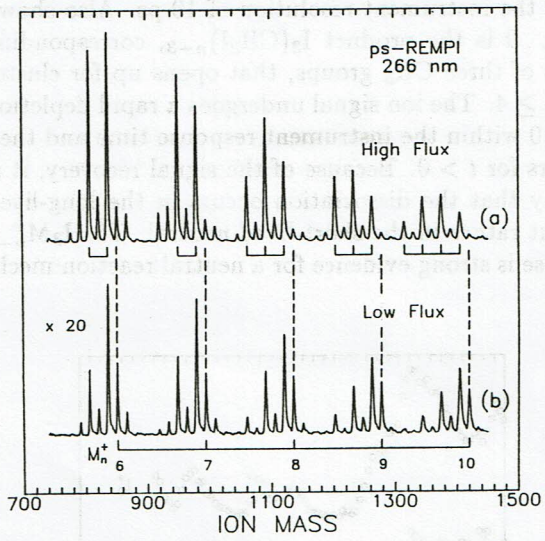

Fig. 10. ps-REMPI mass spectra showing reactions in larger clusters. The 266 nm high and low photon flux conditions differ by about a factor of three (within the range of $10^{27} - 10^{28}$ $cm^{-2}s^{-1}$). The scaling factor in (b) shows that the overall signal intensity is steeply dependent on photon flux, however, the relative intensities are much less sensitive.

CH_3 radical. The photodissociation of CH_3I by 266 nm light provides a 4.66 eV photon to break the 2.30 eV C-I bond. The excess energy in the direct dissociation is released mainly as kinetic energy in the CH_3 radical,[25] which can lead to the exothermic reaction

$$[CH_3 + (CH_3I)_{n-1}] \longrightarrow C_2H_6 + I(CH_3I)_{n-2}$$
$$\Delta H = -1.37\ eV$$

where we assume that the photodissociated I atom is lost (recombination of I atoms would contribute an additional exothermicity of $\Delta H = -1.58$ eV). An alternative pathway to production of ethane would involve the absorption of two photons by $(CH_3I)_n$ to produce two CH_3 radicals that could recombine to release 3.81 eV of heat. In both cases the heat of reaction, which is augmented by the initial radical kinetic energy as well as further recombination including the dissociated I atoms, could drive additional chemistry based on the exothermicity of ethane formation. The hot cluster product above, for example, could undergo the thermal rearrangement

$$I(CH_3I)_{n-2} \longrightarrow C_2H_6 + I_3(CH_3I)_{n-4}$$
$$\Delta H = -0.52\ eV$$

with the additional heat sustaining further loss of ethane. Again subsequent photodissociation would enhance the rate of C-I bond breaking and exothermic production of C_2H_6.

The near absence of a multiple I atom loss product is consistent with efficient caging of this heavy mass which acquires little kinetic energy (0.15-0.25 eV) by photodissociation and even less by the thermal route. This provides an efficient means for production of the major product I_2. The production of I_2 from $(CH_3I)_n$ clusters was first suggested by Vaida *et al.*[24] in work in which they detected I_2^+ by MPI through the valence $\tilde{A}$ state and the Rydberg $\tilde{C}$ state. Their results, however, did not distinguish whether I_2^+ originated from a reaction within a neutral cluster or an ionic cluster. In the present work, the absence of I_2^+ (and $I_2M_{n-2}^+$) by direct high energy EI ionization of $(CH_3I)_n$ and by 266 nm and 532 nm cluster ion photodissociation provides the most compelling evidence for production of $I_2M_{n-2}^+$ by neutral $\tilde{A}$ state cluster reactions. Also in support of a neutral reaction mechanism is the short reaction time ($\leq$ 10 ps), which is consistent with the directly dissociating $\tilde{A}$ state, but not with the lower electronic bound states of the ion.[26]

5. OUTLOOK AND CONCLUSIONS

The combination of picosecond REMPI and direct ion photodissociation studies holds great promise for studying complex reaction mechanisms in size-specific neutral clusters. Although the techniques are now well established for studying stepwise solvation, the work reported here shows that picosecond mass-selective measurements of rapid *intermolecular* photochemistry in clusters offers a new domain for studying the molecular basis of solvation on reactive systems.

6. ACKNOWLEDGEMENTS

I gratefully acknowledge Jhobe Steadman and Eric Fournier for their important contributions to this work. The picosecond clusters program is supported by the Aerospace Sponsored Research program.

7. REFERENCES

1. J. A. Syage, P. M. Felker, and A. H. Zewail, "Picosecond dynamics and isomerization of stilbene in supersonic beams: II. Reaction rates and the potential energy surface," *J. Chem. Phys.* **81**, 4706 (1984).
2. M. Maroncelli, J. MacInnis, and G. R. Fleming, "Polar solvent dynamics and electron-transfer re-

actions," *Science* **243,** 1674 (1989); G. Rothenberger, D. K. Negus, and R. M. Hochstrasser, "Solvent influence on photoisomerization dynamics," *J. Chem. Phys.* **79,** 5360 (1983).

3. O. Cheshnovsky, and S. Leutwyler, "Proton Transfer in neutral gas-phase clusters: α-Naphthol·$(NH_3)_n$," *J. Chem. Phys.* **88,** 4127 (1988).
4. J. F. Garvey and R. B. Bernstein, "Observation of intramolecular ion-molecule reactions within ionized clusters: Hetero systems ...," *J. Am. Chem. Soc.* **109,** 1921 (1987); J. F. Garvey and R. B. Bernstein, "Observation of intramolecular ion-molecule reactions within ionized clusters: The methyl halide systems," *J. Phys. Chem.* **90,** 3577 (1986).
5. J. J. Breen, W. -B. Tzeng, K. Kilgore, R. G. Keesee, and A. W. Castleman, Jr., "Intracluster reactions in phenylacetylene ammonia clusters initiated through resonant enhanced ionization" *J. Chem. Phys.* **90** 19 (1989); O. Echt, P. D. Dao, S. Morgan, and A. W. Castleman, Jr., "Multiphoton ionization of ammonia clusters and the dissociation dynamics of protonated cluster ions," *J. Chem. Phys.* **82** 4076 (1985).
6. B. Brutschy, C. Janes, and J. Eggert, "Intracluster proton-transfer between methylsubstituted benzene cations and polar solvent molecules studied by resonant two-photon ionization," *Ber. Bunsenges, Phys. Chem.* **92,** 74 (1988).
7. J. A. Syage, "Reactivity of aniline cation to stepwise solvation in hydrogen-bonded molecular clusters," *J. Phys. Chem.* **93,** 107 (1989).
8. J. A. Syage, "Photodissociation and metastable decay of solvated cluster ions," *J. Chem. Phys.*, in press (1990).
9. J. Steadman and J. A. Syage, "Picosecond mass-selective measurements of Phenol-$(NH_3)_n$ acid-base chemistry in clusters," *J. Chem. Phys.*, submitted.
10. J. A. Syage and J. Steadman, "Picosecond mass-selective measurements of molecular cluster reactions: $(CH_3I)_n$ $\tilde{A}$ state excitation," *Chem. Phys. Lett.*, in press (1989).
11. J. A. Syage and J. E. Wessel, "Resonant two-photon ionization spectroscopy of naphthalene clusters," *J. Chem. Phys.* **89,** 5962 (1988); J. E. Wessel and J. A. Syage, "Excitonic interactions in naphthalene clusters," *J. Phys. Chem.*, in press (1990).
12. J. A. Syage, "Measurements of electron-impact ionization and dissociation cross sections in a crossed electron-supersonic molecular beam," *Chem. Phys. Lett.* **143,** 19 (1988).
13. J. A. Syage, J. E. Pollard, and J. Steadman, "Resonance ion dissociation spectroscopy of CH_3I^+ produced by molecular beam electron-impact ionization," *Chem. Phys. Lett.* **161,** 103 (1989).
14. J. A. Syage and J. Steadman, "A time-of-flight mass filter for ion and cluster ion photodissociation studies," *Rev. Sci. Instrum.* submitted.
15. C. R. Moylan and J. I. Brauman, "Gas phase acid-base chemistry," *Annu. Rev. Phys. Chem.* **34,** 187 (1983); D. F. McMillen and D. M. Golden, "Hydrocarbon bond dissociation energies," *Annu. Rev. Phys. Chem.* **33,** 493 (1982).
16. P. Kebarle, "Ion thermochemistry and solvation from gas phase ion equilibria," *Annu. Rev. Phys. Chem.* **28,** 445 (1977); M. J. Mautner and C. V. Speller, "Filling of solvent shells about ions. 1. Thermochemical criteria and the effects of isomeric clusters," *J. Phys. Chem.* **90,** 6616 (1986).
17. E. M. Kosower and D. Huppert, "Excited state electron and proton transfers," *Annu. Rev. Phys. Chem.* **37,** 127 (1986).
18. K. K. Smith, K. J. Kaufmann, D. Huppert, and M. Gutman, "Picosecond proton ejection: An ultrafast pH jump," *Chem. Phys. Lett.* **64,** 522 (1979); H. Shizuka, K. Tsutsumi, H. Takeuchi, and I. Tanaka, "Direct measurement of proton dissociation in the excited state of protonated 1-aminopyrene with picosecond pulses," *Chem. Phys. Lett.* **62,** 408 (1979); P. M. Rentzepis and P. F. Barbara, "Proton transfer: A primary picosecond event," *Adv. Chem. Phys.* **47** 627 (1981).
19. E. Pines, D. Huppert, and N. Agmon, "Geminate recombination in excited-state proton transfer reactions: Numerical solution ...," *J. Chem. Phys.* **88,** 5620 (1988); D. H. Huppert, A. Jayaraman, R. G. Maines, Sr., D. W. Steyert, and P. M. Rentzepis, "Effect of pressure on proton transfer rate in aqueous solutions: A picosecond study," *J. Chem. Phys.* **81,** 5596 (1984).
20. S. P. Webb, L. A. Philips, S. W. Yeh, L. M. Tolbert, and J. H. Clark, "Picosecond kinetics of the excited-state, proton-transfer reaction of 1-naphthol in water," *J. Phys. Chem.* **90,** 5154 (1986); J. Lee, R. D. Griffin, and G. W. Robinson, "2-Naphthol: A simple example of proton transfer effected by water structure," *J. Chem. Phys.* **82,** 4920 (1985).
21. D. Solgadi, C. Jouvet, and A. Tramer, "Resonance enhanced multiphoton ionization spectra and ionization thresholds of Phenol-$(NH_3)_n$ clusters," *J. Phys. Chem.* **92,** 3313 (1988).
22. N. Gonohe, H. Abe, N. Mikami, and M. Ito, "Two-color photoionization of van der Waals complexes of fluorobenzene and hydrogen-bond- ed complexes of phenol in supersonic jets," *J. Phys. Chem.* **89,**

3642 (1985).

23. J. L. Knee, L. R. Khundkar, and A. H. Zewail, "Picosecond monitoring of a chemical reaction in molecular beams: Photofragmentation of R-I → $R^{\ddagger}$ + I," *J. Chem. Phys.* **83** 1996 (1985).

24. S. P. Sapers, V. Vaida, and R. Naaman, "Multiphoton ionization study of intra- and intermolecular effects on the photodissociation of methyl iodide," *J. Chem. Phys.* **88** 3638 (1988).

25. R. K. Sparks, K. Shobatake, L. R. Carlson, and Y. T. Lee, "Photofragmentation of CH_3I: Vibrational distribution of the CH_3 fragment," *J. Chem. Phys.* **75** 3838 (1981).

26. D. M. Mintz and T. Baer, Kinetic energy release distributions for the dissociation of internal energy selected CH_3I^+ and CD_3I^+ ions," *J. Chem. Phys.* **65** 2407 (1976); K. Walter, R. Weinkauf, U. Boesl, and E. W. Schlag, K. Walther, R. Weinkauf, U. Boesl, and E. W. Schlag," *J. Chem. Phys.* **89** 1914 (1988).